Enhanced Nonlinear Refractive Index in ϵ-Near-Zero Materials

L. Caspani,[1] R. P. M. Kaipurath,[1] M. Clerici,[1,2] M. Ferrera,[1] T. Roger,[1] J. Kim,[3] N. Kinsey,[3] M. Pietrzyk,[4] A. Di Falco,[4] V. M. Shalaev,[3] A. Boltasseva,[3] and D. Faccio[1,*]

[1]*Institute of Photonics and Quantum Sciences, SUPA, Heriot-Watt University, Edinburgh EH14 4AS, United Kingdom*

[2]*School of Engineering, University of Glasgow, Glasgow G12 8LT, United Kingdom*

[3]*School of Electrical and Computer Engineering and Birck Nanotechnology Center, Purdue University, 1205 West State Street, West Lafayette, Indiana 47907-2057, USA*

[4]*SUPA, School of Physics and Astronomy, University of St. Andrews, St. Andrews KY16 9SS, United Kingdom*

(Received 7 March 2016; published 8 June 2016)

New propagation regimes for light arise from the ability to tune the dielectric permittivity to extremely low values. Here, we demonstrate a universal approach based on the low linear permittivity values attained in the ϵ-near-zero (ENZ) regime for enhancing the nonlinear refractive index, which enables remarkable light-induced changes of the material properties. Experiments performed on Al-doped ZnO (AZO) thin films show a sixfold increase of the Kerr nonlinear refractive index (n_2) at the ENZ wavelength, located in the 1300 nm region. This in turn leads to ultrafast light-induced refractive index changes of the order of unity, thus representing a new paradigm for nonlinear optics.

DOI: 10.1103/PhysRevLett.116.233901

The nonlinear optical response of matter to light is, by its very nature, a perturbative and hence typically weak effect. Applications, e.g., for nonlinear optical switches or quantum optics, are therefore largely underpinned by the continuous endeavor to attain stronger and more efficient light-matter interactions.

Nonlinear mechanisms can typically be classified as resonant or nonresonant, depending on the frequency of light with respect to the characteristic electronic resonances of the material. Nonresonant nonlinearities, like those present in transparent crystals or amorphous materials (e.g., fused silica glass), are generally weak and require high light intensities and/or very long samples to take advantage of an extended light-matter interaction. Conversely, resonant nonlinearities can be several orders of magnitude stronger, but this comes at the price of introducing detrimental losses. A typical example is that of metals, which both reflect and absorb light strongly [1–3]. An alternative approach to enhancing the nonlinear response of a material consists of creating artificial electromagnetic resonances, for example, by stacking materials of different refractive indices or using other types of composite materials [4–11]. Creating resonant metal-dielectric stacks and composites yields a very strong nonlinear enhancement [12–14], but it inevitably exacerbates the detrimental role of linear and nonlinear losses.

Here, we propose a different approach to enhancing the effective nonlinearity without resorting to optical resonances. Our approach relies on enhancing the nonlinear effect, measured in terms of the nonlinear Kerr index n_2, rather than on a direct enhancement of the intrinsic $\chi^{(3)}$ nonlinear susceptibility. As we show below, this enhancement arises due to the fact that the nonlinear refractive index is a function of both the nonlinear susceptibility and the linear refractive index. Recent progress in material design and fabrication has provided access to the full range of linear optical properties bounded by dielectric and metallic regimes. Of particular relevance for this Letter are materials which exhibit a real part of the dielectric permittivity that is zero, or close to zero, such as transparent conducting oxides where their permittivity crossover is typically located in the near infrared spectral region.

The linear properties of these "ϵ-near-zero" (ENZ) materials have been investigated [15–32] for applications ranging from controlling the radiation pattern of electromagnetic sources to novel waveguiding regimes and perfect absorption. Similarly, the nonlinear properties have also been shown to be largely affected by the ENZ condition [33–40], and recently it has been theoretically predicted that the interplay between linear and nonlinear properties of ENZ bulk materials may allow three-dimensional self-trapping of light [41]. However, experimental evidence reported so far is limited to phase matching-free conditions in four-wave mixing [42], enhanced third and second harmonic generation [43–45], and ultrafast optical switching [46].

In order to illustrate how the nonlinear Kerr index may be enhanced as a result of the ENZ *linear* properties, we employed a 900 nm thick film of oxygen-deprived aluminium-doped zinc oxide (AZO) [46,47]. The AZO 900 nm thick thin film was deposited by pulsed laser deposition (PVD Products, Inc.) [48,49] using a KrF excimer laser (Lambda Physik GmbH) operating at a wavelength of 248 nm for source material ablation (see Ref. [47] for more details).

The linear response, i.e., the real and imaginary parts of ϵ, ϵ_r and ϵ_i, respectively, were measured by a standard

reflection and transmission measurement using a tunable-wavelength, 100 fs, 100 Hz repetition rate weak probe beam; see Figs. 1(a) and 1(b). The linear permittivity, shown in Fig. 1(c), is then evaluated from the reflection and transmission measurements by means of an inverse transfer matrix approach: this allows us to evaluate the complex permittivity from the measured reflectivity and transmissivity. The condition $\varepsilon_r = 0$ (ENZ wavelength) is achieved at ~1300 nm.

For many applications and measurements, the nonlinear Kerr index n_2 is used instead of the third-order nonlinear $\chi^{(3)}$ tensor. For the case involving a nondegenerate pump-probe scenario with a weak probe and an intense pump beam, the nonlinear index is given by [50]

$$n_2 = \frac{3}{2\varepsilon_0 c}\frac{\chi^{(3)}}{n_r^{\text{pump}}(n_r + in_i)}, \tag{1}$$

where both n_2 and $\chi^{(3)}$ are complex quantities, ϵ_0 is the vacuum permittivity, c is the speed of light in vacuum, $n_{r,i}$ are the real and imaginary parts of the linear refractive index at the weak probe wavelength, and n_r^{pump} is the real part of the refractive index at the pump wavelength.

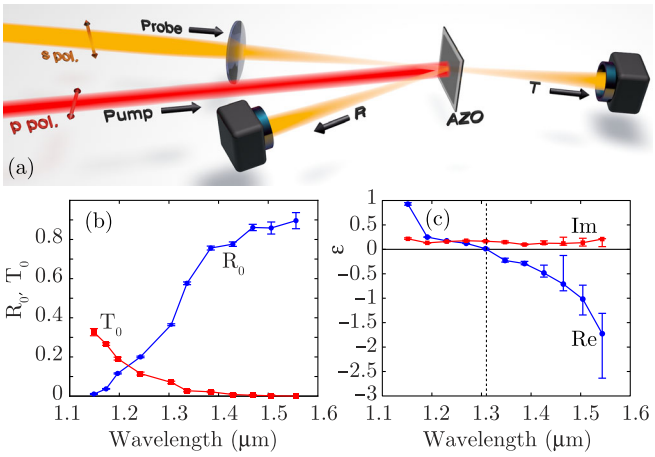

FIG. 1. (a) Experimental setup. A high intensity, horizontally polarized beam at 785 nm pumps the thin AZO film at normal incidence. The reflection and transmission of a weak probe beam (variable wavelength between 1150 and 1550 nm, vertically polarized, ~10° angle of incidence) are simultaneously recorded. For the linear characterization, the pump beam was blocked. (b) Measured reflectivity (R_0, blue circles) and transmissivity (T_0, red squares) in the linear regime (no pump beam). The error bars have been evaluated as the standard deviation on a sample of 300 measurements. (c) Real (blue circles) and imaginary (red squares) part of the linear permittivity extracted from the data in (a) using an inverse transfer matrix approach. The error bars have been evaluated by extracting ϵ from the pairs $\{R_0 + \sigma_{R_0}, T_0 + \sigma_{T_0}\}$ (upper bounds) and $\{R_0 - \sigma_{R_0}, T_0 - \sigma_{T_0}\}$ (lower bounds), where σ_{R_0} and σ_{T_0} are the reflectivity and transmissivity standard deviations, respectively. The large error bars for the real part of the permittivity at longer wavelengths are due to the very low values of transmissivity measured, in turn resulting in a high relative error.

The pump-induced nonlinear refractive index change is then given by $\delta n = n_2 I$, where I is the intensity of the optical beam [50].

We note that although it is generally desirable to minimize the absorption losses, the imaginary part of the material's linear response also plays a crucial role in determining the effective nonlinear response. This can be appreciated by separating the complex nonlinear Kerr index into its real and imaginary parts [51]:

$$n_{2r} = \frac{3}{2\varepsilon_0 c}\frac{n_r\chi_r^{(3)} + n_i\chi_i^{(3)}}{D} \tag{2}$$

$$n_{2i} = \frac{3}{2\varepsilon_0 c}\frac{n_r\chi_i^{(3)} - n_i\chi_r^{(3)}}{D}, \tag{3}$$

where $D = n_r^{\text{pump}}(n_r^2 + n_i^2)$. The imaginary part n_{2i} is usually associated with what is known as the nonlinear absorption coefficient, $\beta_2 = 4\pi n_{2i}/\lambda$, where λ is the vacuum wavelength. Consequently, we see that it is the interplay between linear (n_r, n_i) and nonlinear ($\chi_r^{(3)}$, $\chi_i^{(3)}$) properties that defines the nonlinear index and provides a means for enhancing or tailoring the effective n_{2r} and β_2 coefficients as a function of wavelength.

An insight on the underlying physical mechanism at play can be gained with the simplified model $\chi_r^{(3)} = \chi_i^{(3)} = \text{const}$, which allows us to predict the n_2 and β_2 behavior based only on the linear material properties. In this case, the wavelength dependence of n_{2r} is determined by the term $(n_r + n_i)/D$, whereas the nonlinear absorption coefficient is determined by $(n_r - n_i)/D$. Both of these quantities are plotted, in Figs. 2(a) and 2(b), respectively, starting with the measured frequency-dependent linear refractive index of our sample.

The presence of an ENZ wavelength (indicated by the vertical dashed line) significantly modifies the behavior of the materials: a peak is observed in the $(n_r + n_i)/D$ term, indicating an enhancement of n_{2r}, while the nonlinear absorption shows a more complex behavior and changes

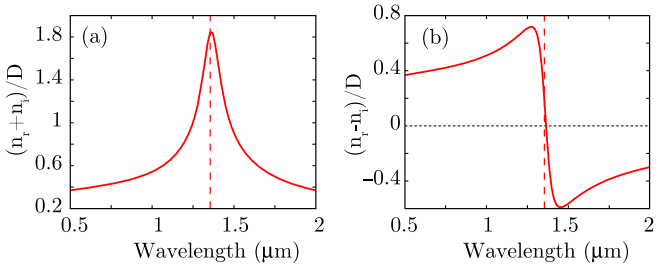

FIG. 2. Plots of the theoretically estimated trends for n_2 and β_2 from Eqs. (2) and (3). (a) Plot of $(n_r + n_i)/D$ with $D = n_r^{\text{pump}}(n_r^2 + n_i^2)$. This term weighs the real part of the nonlinearity, n_{2r}. (b) Plot of $(n_r - n_i)/D$. This term weighs the imaginary part of the nonlinearity, β_2. The vertical dashed lines indicate the ENZ wavelength.

sign. The transition from positive to negative (i.e., saturable) nonlinear absorption occurs at the ENZ wavelength, such that the maximum nonlinear phase shift can be attained with zero nonlinear losses. This is a unique feature of ENZ materials and underlines the crucial role played by the material's linear dispersion and the effects of the ENZ condition on the nonlinear optical response. As discussed below, the condition $\chi_r^{(3)} = \chi_i^{(3)}$ is not strictly required for observing the n_2 enhancement at the ENZ condition.

We note that, in order to observe the described enhancement, one needs to achieve the ENZ condition for the real part of the linear dielectric permittivity while maintaining a relatively low imaginary part, as this in turn guarantees a low real part of the refractive index. The AZO film employed here displays all of the required properties for both the linear and nonlinear susceptibility to experimentally demonstrate the predicted nonlinear enhancement. Remarkably, this also comes with an extremely high damage threshold—no damage was observed up to 2 TW/cm^2 (at 785 nm, 100 Hz repetition rate), as compared to the few GW/cm^2 typical of metallic structures.

We characterized the nonlinear response of the AZO film with a pump and probe system [Fig. 1(a)] by measuring the pump-induced change in reflectivity and transmissivity for different pump intensities; see Figs. 3(a) and 3(b). We observe a large variation in the reflectivity around the ENZ wavelength. Conversely, the highest values of relative transmissivity change are observed for longer wavelengths, which is simply due to the normalization with respect to the initial transmission T_0 that is very close to zero in this spectral region.

The pump pulse (100 fs, 100 Hz repetition rate, horizontally polarized) has a fixed wavelength $\lambda_{\text{pump}} =$ 785 nm and is at normal incidence with respect to the sample. The probe pulse (100 fs, 100 Hz repetition rate, vertically polarized) from an optical parametric amplifier and tunable from 1150 to 1550 nm is incident at a small ($< 10°$) angle. The intensity of the probe beam is kept low

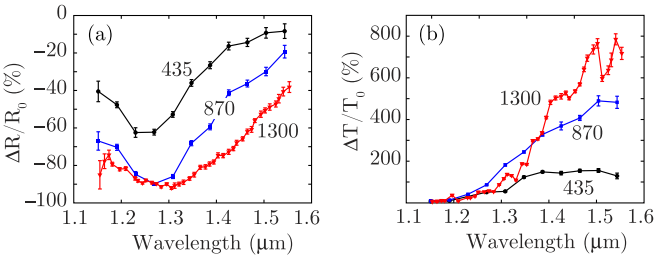

FIG. 3. (a) Measured reflectivity change $\Delta R/R_0 = (R - R_0)/R_0$, where R is the reflectivity at the probe wavelength with the pump and R_0 is the linear value (pump off) for increasing pump intensities: $I_p = 435$ GW/cm^2 (the black circles), $I_p =$ 870 GW/cm^2 (the blue squares), and $I_p = 1300$ GW/cm^2 (the red triangles). (b) Same as (a) but for transmissivity change $\Delta T/T_0 = (T - T_0)/T_0$. The error bars have been evaluated by propagating the error of the R, R_0, T, and T_0 standard deviations, from a sample of 300 measurements.

(below the GW/cm^2 level) to avoid any nonlinearity from the probe itself (no change in the probe transmissivity and reflectivity was observed at this intensity). The probe beam waist ($w_{0,\text{probe}} = 45$ μm) is smaller than the pump beam waist ($w_{0,\text{pump}} = 125$ μm), in order to obtain a uniform pump intensity across the probe beam. For all of the measurements, the pump beam size was constant and the intensity was changed only by increasing the energy. The pump-probe delay was then optimized to maximize the nonlinear effect.

For each probe wavelength, we measure the pump-induced change in the reflection and transmission of the probe beam, then use these values to retrieve the permittivity in the pumped case (ε_{nl}) by applying an inverse transfer matrix approach. Whenever the dependence of ε_{nl} from I_p is linear, we may determine the third-order nonlinearity from the relation [52]:

$$\chi^{(3)}(\omega_p, \omega_{\text{probe}}) = \frac{n_r^{\text{pump}} \varepsilon_0 c}{3} \frac{\partial \varepsilon_{\text{nl}}(\omega_{\text{probe}}, I_p)}{\partial I_p}, \qquad (4)$$

where ω_p and I_p are the pump frequency and intensity, respectively, and the derivative can be evaluated as the slope of the linear fit of $\varepsilon_{\text{nl}}(I_p)$. In Fig. 4(a) we show an example of $\varepsilon_{\text{nl}}(I_p)$ for a specific probe wavelength ($\lambda_{\text{probe}} = 1258$ nm), with the corresponding linear fit, while Fig. 4(b) reports the resulting real and imaginary parts of the material $\chi^{(3)}$ as a function of the probe wavelength.

From the $\chi^{(3)}$ values, it is possible to extract the nonlinear Kerr index by exploiting the formulas in Eqs. (2) and (3). The results for both the real part, n_{2r}, and the nonlinear absorption coefficient, β_2, are presented in Figs. 5(a) and 5(b), and they show a good qualitative agreement with the theoretical curves in Fig. 2. Most importantly, as seen in Fig. 5(a), a clear sixfold enhancement of $n_{2,r}$ (with respect to its lowest value at 1152 nm) is observed around the ENZ wavelength. To further support our analysis, we compare the theoretical predictions with the experimental results in Fig. 5. The red lines in Figs. 5(a) and 5(b) show the expected values of n_{2r} and β_2 obtained from the measured

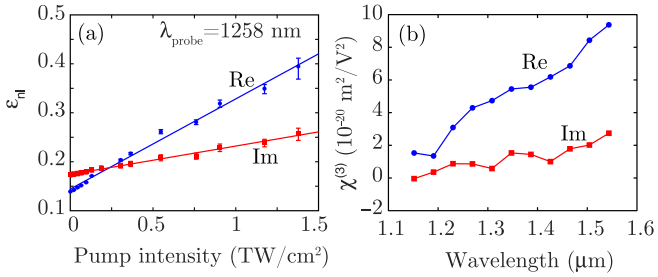

FIG. 4. (a) Real (blue circles) and imaginary (red squares) part of ε_{nl} as a function of the pump intensity for a specific probe wavelength, and corresponding linear fits (the solid lines). (b) Real (blue circles) and imaginary (red squares) part of the $\chi^{(3)}$ tensor for different probe wavelengths.

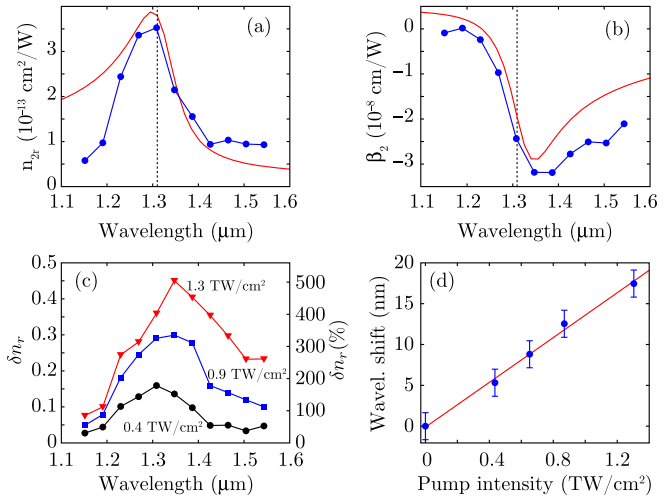

FIG. 5. (a) Real part of the nonlinear Kerr index, n_{2r}, and (b) nonlinear absorption coefficient, $\beta_2 = 4\pi n_{2i}/\lambda$, obtained from Eq. (2) and the data in Fig. 4 (the blue dots). The red lines represent the expected theoretical result obtained from Eq. (6). (c) Change in the real part of the refractive index, $\delta n_r = n_r(I_p) - n_r(I_p = 0)$, for different pump intensities (the left axis). Maximum relative refractive index change, $\delta n_r/n_r(I_p = 0)$, at 1390 nm (the right axis). (d) Measured shift of the probe carrier wavelength as a function of the pump intensity (the red curve is the linear fit).

linear refractive index and assuming a nondispersive $\chi^{(3)}$ with comparable real and imaginary parts. In detail, we plot the quantities:

$$n_{2r,\mathrm{theor}} = \frac{3}{2\varepsilon_0 c}\frac{n_r A + n_i B}{n_r^{\mathrm{pump}}(n_r^2 + n_i^2)} \tag{5}$$

$$\beta_{2,\mathrm{theor}} = \frac{4\pi}{\lambda}\frac{3}{2\varepsilon_0 c}\frac{n_r B - n_i A}{n_r^{\mathrm{pump}}(n_r^2 + n_i^2)}, \tag{6}$$

where A and B (representing $\chi_r^{(3)}$ and $\chi_i^{(3)}$, respectively) are used as fitting parameters and $A = 4 \times 10^{-20}$ m^2/V^2 and $B = 1 \times 10^{-20}$ m^2/V^2. The relatively good agreement with the data shows that, indeed, our measurements are compatible with the assumption used in Fig. 2, i.e., $\chi_r^{(3)} \sim \chi_i^{(3)} = \mathrm{const}$.

Remarkably, for the laser pulse intensities used in our experiments, the measured nonlinear refractive index n_{2r} gives a change of refractive index in the medium ($\delta n_r = n_{2r} I_p$) that is of the order of the linear refractive index.

For example, at 1390 nm we measured a change of refractive index as high as $\delta n_r = 0.4$, as compared to the linear index $n_r = 0.09$, recorded for the highest intensity, $I_p = 1300$ GW/cm^2, without observing any optical damage; see Fig. 5(c). This large modulation places the ENZ nonlinearity in AZO in a regime where the approximation of expanding the material polarization in a power series breaks down [50].

We note that similar results are, in principle, expected in any medium displaying similar linear properties together with a weak $\chi^{(3)}$ dispersion and for $\chi_r^{(3)} \sim \chi_i^{(3)}$. Most importantly, the ENZ condition is often achieved together with significant losses, while AZO films are featured in the ENZ condition combined with a relatively low imaginary part of the permittivity, ε_i. The latter condition ensures that the linear refractive index is significantly close to zero, which, as discussed above, maximizes the observed enhancement of the nonlinear index.

Finally, in Fig. 5(d) we show how the carrier wavelength of the probe pulse transmitted through the sample increases linearly with the pump intensity and shifts up to 17.5 ± 1.6 nm, i.e., by more than the 15 nm probe input bandwidth. This "nanoscale wavelength shifter" could be applied, e.g., for single photon wavelength division multiplexing [53]. In our demonstration, large frequency shifts were achieved with high pump intensities (TW/cm^2), which might, however, be reduced by relying on nanostructured materials [54].

In conclusion, ENZ materials allow one to tailor and access novel linear propagation regimes. Here, we have shown the ability to exploit the ENZ regime for enhancing third-order nonlinear effects, thus leading to an ultrafast light-induced metal-to-dielectric phase change. The interplay between the real and imaginary parts of the linear refractive index and the $\chi^{(3)}$ tensor also leads to a peculiar wavelength-dependent behavior of the nonlinear refractive index. This allows, for example, an enhancement of the real part of the nonlinear index, which in turn is associated with a nonlinear phase shift in the probe beam. On the other hand, novel and interesting behaviors are observed, such as the change in sign of the β_2 coefficient, effectively eliminating nonlinear absorption close to the ENZ wavelength. Moreover, the possibility of optically controlling the material's refractive index by amounts comparable to the linear values (close to 500% of the relative changes in the refractive index are reported here) may allow one to effectively tailor the impedance of the material and match it to that of the surrounding medium. The ability to access ultrafast light-induced refractive index changes of the order of unity represents a new paradigm for nonlinear optics.

All data relevant to this work may be obtained at [55].

L. C. and M. F. acknowledge the support from the People Programme (Marie Curie Actions) of the European Union's FP7 Programme under REA Grant Agreements No. 627478 (THREEPLE) and No. 329346 (ATOMIC), respectively. J. K., N. K., V. M. S., and A. B. wish to acknowledge support from AFOSR MURI Grant No. FA9550-14-1-0389, AFOSR Grant No. FA9550-14-1-0138, and NSF MRSEC Grant No. DMR-1120923. D. F. acknowledges financial support from the European Research Council under the European Union Seventh Framework Programme

(FP/2007-2013)/ERC GA 306559 and EPSRC (UK, Grant No. EP/M009122/1).

Note added.—Recently, we became aware of a related study that has now been published [56].

*d.faccio@hw.ac.uk

[1] D. Ricard, P. Roussignol, and C. Flytzanis, Opt. Lett. **10**, 511 (1985).
[2] D. T. Owens, C. Fuentes-Hernandez, J. M. Hales, J. W. Perry, and B. Kippelen, J. Appl. Phys. **107**, 123114 (2010).
[3] R. W. Boyd, Z. Shi, and I. D. Leon, Opt. Commun. **326**, 74 (2014).
[4] I. I. Smolyaninov, A. V. Zayats, and C. C. Davis, Phys. Rev. B **56**, 9290 (1997).
[5] J. Renger, R. Quidant, N. van Hulst, and L. Novotny, Phys. Rev. Lett. **104**, 046803 (2010).
[6] M. I. Stockman, D. J. Bergman, C. Anceau, S. Brasselet, and J. Zyss, Phys. Rev. Lett. **92**, 057402 (2004).
[7] A. Bouhelier, M. Beversluis, A. Hartschuh, and L. Novotny, Phys. Rev. Lett. **90**, 013903 (2003).
[8] S. Kim, J. Jin, Y.-J. Kim, I.-Y. Park, Y. Kim, and S.-W. Kim, Nature (London) **453**, 757 (2008).
[9] K. D. Ko, A. Kumar, K. H. Fung, R. Ambekar, G. L. Liu, N. X. Fang, and K. C. Toussaint, Jr., Nano Lett. **11**, 61 (2011).
[10] R. W. Boyd and J. E. Sipe, J. Opt. Soc. Am. B **11**, 297 (1994).
[11] V. M. Shalaev, *Nonlinear Optics of Random Media: Fractal Composites and Metal-Dielectric Films*, Springer Tracts in Modern Physics (Springer-Verlag, Berlin, 2000).
[12] N. N. Lepeshkin, A. Schweinsberg, G. Piredda, R. S. Bennink, and R. W. Boyd, Phys. Rev. Lett. **93**, 123902 (2004).
[13] G. L. Fischer, R. W. Boyd, R. J. Gehr, S. A. Jenekhe, J. A. Osaheni, J. E. Sipe, and L. A. Weller-Brophy, Phys. Rev. Lett. **74**, 1871 (1995).
[14] P. Farah, N. Gibbons, F. M. Huang, and J. J. Baumberg, Phys. Rev. B **84**, 125442 (2011).
[15] A. Alù, M. G. Silveirinha, A. Salandrino, and N. Engheta, Phys. Rev. B **75**, 155410 (2007).
[16] B. Edwards, A. Alù, M. E. Young, M. Silveirinha, and N. Engheta, Phys. Rev. Lett. **100**, 033903 (2008).
[17] R. W. Ziolkowski, Phys. Rev. E **70**, 046608 (2004).
[18] H. Zhou, S. Qu, Z. Pei, Y. Yang, J. Zhang, J. Wang, H. Ma, C. Gu, X. Wang, Z. Xu, W. Peng, and P. Bai, J. Electromagn. Waves Appl. **24**, 1387 (2010).
[19] J. Yang, M. Huang, and J. Peng, Radioengineering **18**, 124 (2009).
[20] J. Soric, N. Engheta, S. Maci, and A. Alù, IEEE Trans. Antennas Propag. **61**, 33 (2013).
[21] Y. Jin and S. He, Opt. Express **18**, 16587 (2010).
[22] M. Silveirinha and N. Engheta, Phys. Rev. Lett. **97**, 157403 (2006).
[23] M. Silveirinha and N. Engheta, Phys. Rev. B **75**, 075119 (2007).
[24] Y. Pan and S. Xu, IET Microwaves Antennas Propag. **3**, 821 (2009).
[25] A. Alù and N. Engheta, IEEE Trans. Antennas Propag. **58**, 328 (2010).
[26] V. C. Nguyen, L. Chen, and K. Halterman, Phys. Rev. Lett. **105**, 233908 (2010).
[27] S. Feng, Phys. Rev. Lett. **108**, 193904 (2012).
[28] R. Fleury and A. Alù, Phys. Rev. B **87**, 201101 (2013).
[29] R. Maas, J. Parsons, N. Engheta, and A. Polman, Nature Photon. **7**, 907 (2013).
[30] T. S. Luk, S. Campione, I. Kim, S. Feng, Y. C. Jun, S. Liu, J. B. Wright, I. Brener, P. B. Catrysse, S. Fan, and M. B. Sinclair, Phys. Rev. B **90**, 085411 (2014).
[31] J. Yoon, M. Zhou, M. A. Badsha, T. Y. Kim, Y. C. Jun, and C. K. Hwangbo, Sci. Rep. **5**, 12788 (2015).
[32] T. Y. Kim, M. A. Badsha, J. Yoon, S. Y. Lee, Y. C. Jun, and C. K. Hwangbo, Sci. Rep. **6**, 22941 (2016).
[33] C. Argyropoulos, P.-Y. Chen, G. D'Aguanno, N. Engheta, and A. Alù, Phys. Rev. B **85**, 045129 (2012).
[34] A. Ciattoni, C. Rizza, and E. Palange, Phys. Rev. A **81**, 043839 (2010).
[35] M. A. Vincenti, D. de Ceglia, A. Ciattoni, and M. Scalora, Phys. Rev. A **84**, 063826 (2011).
[36] D. de Ceglia, S. Campione, M. A. Vincenti, F. Capolino, and M. Scalora, Phys. Rev. B **87**, 155140 (2013).
[37] C. Rizza, A. Ciattoni, and E. Palange, Phys. Rev. A **83**, 053805 (2011).
[38] A. Ciattoni, C. Rizza, and E. Palange, Opt. Express **18**, 11911 (2010).
[39] M. Kauranen and A. V. Zayats, Nature Photon. **6**, 737 (2012).
[40] C. Rizza, A. Di Falco, and A. Ciattoni, Appl. Phys. Lett. **99**, 221107 (2011).
[41] A. Marini and F. J. García de Abajo, Sci. Rep. **6**, 20088 (2016).
[42] H. Suchowski, K. O'Brien, Z. J. Wong, A. Salandrino, X. Yin, and X. Zhang, Science **342**, 1223 (2013).
[43] A. Capretti, Y. Wang, N. Engheta, and L. D. Negro, Opt. Lett. **40**, 1500 (2015).
[44] T. S. Luk, D. de Ceglia, S. Liu, G. A. Keeler, R. P. Prasankumar, M. A. Vincenti, M. Scalora, M. B. Sinclair, and S. Campione, Appl. Phys. Lett. **106**, 151103 (2015).
[45] A. Capretti, Y. Wang, N. Engheta, and L. Dal Negro, ACS Photonics **2**, 1584 (2015).
[46] N. Kinsey, C. DeVault, J. Kim, M. Ferrera, V. M. Shalaev, and A. Boltasseva, Optica **2**, 616 (2015).
[47] G. V. Naik, J. Liu, A. V. Kildishev, V. M. Shalaev, and A. Boltasseva, Proc. Natl. Acad. Sci. U.S.A. **109**, 8834 (2012).
[48] A. V. Singh, R. M. Mehra, N. Buthrath, A. Wakahara, and A. Yoshida, J. Appl. Phys. **90**, 5661 (2001).
[49] H. Kim, J. Horwitz, S. Qadri, and D. Chrisey, Thin Solid Films **420–421**, 107 (2002).
[50] R. Boyd, *Nonlinear Optics* (Academic Press, New York, 2008).
[51] D. D. Smith, Y. Yoon, R. W. Boyd, J. K. Campbell, L. A. Baker, R. M. Crooks, and M. George, J. Appl. Phys. **86**, 6200 (1999).
[52] R. M. Kaipurath, M. Pietrzyk, L. Caspani, T. Roger, M. Clerici, C. Rizza, A. Ciattoni, A. Di Falco, and D. Faccio, Sci. Rep. **6**, 27700 (2016).
[53] N. Matsuda, Sci. Adv. **2**, e1501223 (2016).
[54] M. Abb, Y. Wang, C. H. de Groot, and O. L. Muskens, Nat. Commun. **5**, 4869 (2014).
[55] DOI: 10.17861/d82f29dc-5c47-4c5a-b893-c1ea93ab5224.
[56] M. Z. Alam, I. De Leon, and R. W. Boyd, Science **352**, 795 (2016).